STORM STUDIES IN THE ARCTIC (STAR)

BY JOHN HANESIAK, RONALD STEWART, PETER TAYLOR, KENT MOORE, DAVID BARBER, GORDON MCBEAN, WALTER STRAPP, MENGISTU WOLDE, RON GOODSON, EDWARD HUDSON, DAVID HUDAK, JOHN SCOTT, GEORGE LIU, JUSTIN GILLIGAN, SUMITA BISWAS, DANIELLE DESJARDINS, ROBYN DYCK, SHANNON FARGEY, ROBERT FIELD, GABRIELLE GASCON, MARK GORDON, HEATHER GREENE, CARLING HAY, WILLIAM HENSON, KLAUS HOCHHEIM, ALEX LAPLANTE, REBEKAH MARTIN, MARNA ALBARRAN MELZER, AND SHUNLI ZHANG

With 14 research flights from Baffin Island, surface- and satellite-based instruments, STAR aims to improve understanding and prediction of severe arctic storms and their hazards

Storms and their related hazards over the Arctic have profound effects, including loss of life and influences on industry, transportation, hunting, recreation, and the landscape itself (terrestrial, sea ice, and ocean). Over the past few decades, there has been evidence that the occurrence of extreme storms has increased (Stone et al. 2000; McCabe et al. 2001; Zhang et al. 2004) as well as their associated hazardous weather in some regions (Hanesiak and Wang 2005). Extreme weather directly affects the lives of communities and individuals living in the Canadian Arctic (e.g. NTI 2001; Hassol 2004). According to the *Nunatsiaq News* (5 April 2005), "erratic weather and changing ice patterns are leaving more Nunavik hunters stranded out on the land without traditional techniques to help them."

There are several recent examples of extreme weather events that have occurred in the southeast Arctic alone. In February 2006, warm temperatures (>5°C compared to a normal of –20°C) and rain showers occurred in association with an intense cyclone across south Baffin Island, breaking records in the Nunavut Territory. Icy conditions on runways grounded aircraft in Iqaluit (the capital city of Nunavut, with a population of more than 10,000) and 125 km h^{-1} winds destroyed one building and broke windows in Pangnirtung, Nunavut (*Nunatsiaq News*, 3 March 2006, and *CBC*, 28 February 2006). Another recent storm (7–8 June 2008) produced ▶

Ground blowing snow event during STAR at the primary meteorological installation in Iqaluit, Nunavut, Canada. (Photo: Peter Taylor)

unprecedented heavy rain and flash flooding in Pangnirtung, Nunavut, that caused extensive soil erosion and washed out a major community bridge, stranding 200 residents (*Canadian Press*, 17 June 2008). Several housing units were nearly lost as a result of the erosion. The event was caused by heavy rain in association with unusually warm temperatures (more than 7°C above the normal daytime maximum) that caused rapid snowmelt in the higher terrain. A record-breaking wind event took place in Iqaluit, Nunavut, in February 2007. Winds gusting up to 140 km h^{-1} caused extensive damage to the high school and an 8-story building by blowing off entire sections of their roofs (Neilsen 2007). Strong wind events are not uncommon in the Arctic; however, it is anticipated that more extreme weather events such as these will become more prevalent.

Only one major Canadian-led experiment has focused on arctic storms—the 1994 Beaufort and Arctic Storms Experiment (BASE; Hudak et al. 1995; Hanesiak et al. 1996)—although the Mackenzie Global Energy and Water Cycle Experiment (GEWEX) Study (MAGS) also carried out some storm observations (Stewart et al. 1998). BASE and MAGS took place in the lee of the Western Cordillera, which significantly influence storm systems. For example, Hanesiak et al. (1996) used aircraft and other field observations from BASE to study a high-latitude warm front and found that the overall structure of the warm front and surrounding region were similar to those of midlatitude storms; however, the precipitation rates, liquid water content (LWC), horizontal and vertical winds, turbulence, and thermal advection were generally weaker than those of the midlatitude counterparts. A steep frontal region resulted from strong Coriolis influences, limiting the amount of cloud and precipitation ahead of the system. In addition, mesoscale frontogenic forcing was primarily controlled by the tilting of isentropic surfaces with confluence/convergence being a secondary influence. Using a 2D cloud-resolving model, Szeto et al. (1997) found that many of the structural characteristics of a high-latitude frontal system were the consequences of the subfreezing temperatures and enhanced planetary rotation in the region. The precipitation efficiency of a system is decreased (increased) when the background static stability is increased (decreased) or when the Coriolis parameter is increased (decreased) (Szeto et al. 1997). Hudak et al. (2004) and Stewart et al. (2004) used a variety of field observations during MAGS to characterize cloud and precipitation systems transiting the western Canadian Arctic. Unique features included the prevalence of multilayered systems, the cold temperatures of low clouds, significant sublimation effects, and significant diurnal trends in cloud properties in winter. They also noted that weather prediction models needed to be improved in simulating these characteristics.

Another Arctic project was the First International Satellite Cloud Climatology Project (ISCCP) Regional Experiment–Arctic Cloud Experiment (FIRE–ACE), which took place in 1998 in the western Canadian Arctic (Curry 2001). This project, however, was not primarily focused on storms but rather on cloud characteristics/microphysics in relation to radiation. Although not conducted in the Arctic, information from the 1986 and 1992 Canadian Atlantic Storms Program (CASP) field experiments that took place in Atlantic Canada is also relevant (see, e.g., Stewart 1991; Hanesiak and Stewart 1995). Many studies launched from the CASP projects, including the development of conceptual storm models and research into strong winds and low-level jet characteristics, rain–snow boundary structures, and internal feedbacks, and heavy precipitation.

AFFILIATIONS: Hanesiak, Stewart, Barber, Liu, Gilligan, Desjardins, Dyck, Fargey, Hochheim, and Martin—Department of Environment and Geography, University of Manitoba, Winnipeg, Manitoba, Canada; Taylor, Biswas, Gordon, and Melzer—Department of Earth and Space Science, York University, Toronto, Ontario, Canada; Moore, Field, Hay, and Zhang—Department of Physics, University of Toronto, Ontario, Toronto, Canada; McBean—Department of Geography, University of Western Ontario, London, Ontario, Canada; Strapp, Hudak, and Scott—Cloud Physics and Severe Weather Research Section, Environment Canada, Toronto, Ontario, Canada; Wolde—Flight Research Laboratory, National Research Council of Canada, Ottawa, Ontario, Canada; Goodson—Hydrometeorology and Arctic Laboratory, Environment Canada, Edmonton, Alberta, Canada; Hudson—Prairie and Arctic Storm Prediction Centre, Environment Canada, Edmonton, Alberta, Canada; Gascon, Greene, Henson, and Laplante—Department of Atmospheric and Ocean Sciences, McGill University, Montreal, Quebec, Canada
CORRESPONDING AUTHOR: John Hanesiak, Department of Environment and Geography, University of Manitoba, Rm. 440, Wallace Bldg., 125 Dysart Rd., Winnipeg, MB R3T 2N2, Canada
E-mail: john_hanesiak@umanitoba.ca

The abstract for this article can be found in this issue, following the table of contents.
DOI:10.1175/2009BAMS2693.1

In final form 24 June 2009

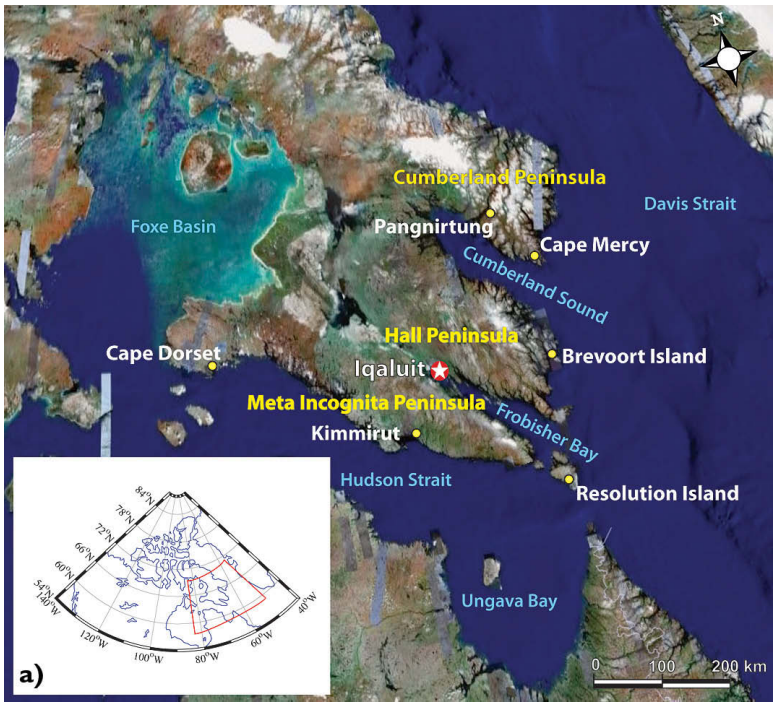

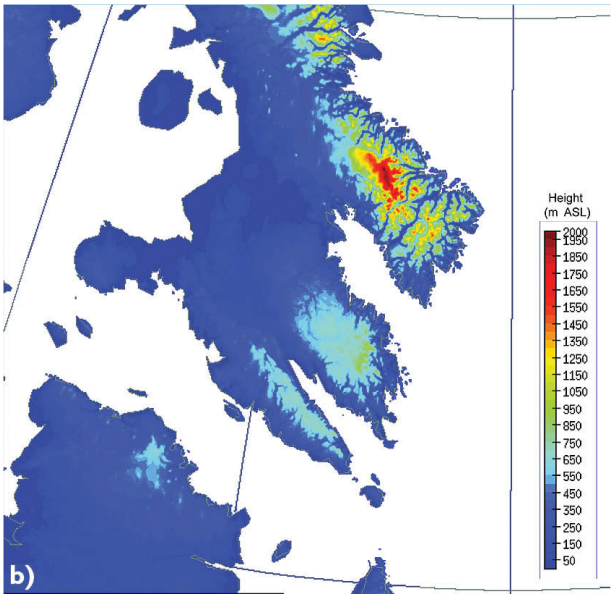

Fig. 1. (a) Geography of the STAR project area as well as standard Environment Canada hourly surface weather reporting stations (in white text). The inset shows the entire Canadian Arctic region for perspective. Iqaluit is at the northeast end of Frobisher Bay and Pangnirtung within Cumberland Sound—the two primary sites where detailed STAR surface and upper-air observations were taken. (b) Topographic map of southern Baffin Island [color legend indicates MSL height (m)]. The map also signifies the domain and topography of the 2.5-km-resolution GEM-LAM.

Despite the economic, environmental, climatic, and societal effects of arctic storms and their related hazards, there has been no coordinated and integrated research program addressing these issues in Canada. The deficiency in our understanding of storms was confirmed in a recent assessment of the current state of knowledge about climate change and its effects in northern Canada, undertaken by the Northern Climate Exchange (see www.taiga.net/nce/). The Arctic Climate Impact Assessment (ACIA) International Scientific Symposium held in Reykjavik, Iceland, in November 2004 highlighted significant changes in arctic weather and climate patterns and a need for more research into extreme and adverse weather and climate processes. This would include high-resolution modeling and detailed field experiments and validation (Hassol 2004).

Some of the most intense arctic storms occur in the eastern Canadian Arctic (Fig. 1). Extratropical and mesoscale cyclones are often observed to transit the region, especially during the spring and autumn seasons when the major North Atlantic storm track is situated just to the south of Baffin Island. As low pressure systems move in from the west and south, they often intensify as they track east and north (e.g., Hudson et al. 2001; Hoskins and Hodges 2002; Intihar and Stewart 2005). Some research has been devoted to this part of the Arctic, examining the general character of such storms and their precipitation features (e.g., Roberts et al. 2008; Roberts and Stewart 2008); however, limited detailed field data have been available. The interaction of these low pressure systems with local topography is critical to understanding local and regional weather (see the "Project area, climatology, and instrumentation" section for a more detailed climatological discussion).

The Storm Studies in the Arctic (STAR) project (www.starnetwork.ca) focuses on arctic storms over the southern Baffin Island region, primarily because of existing observational infrastructure and significant population density. Iqaluit, located on southern Baffin Island, is a thriving city with an increasing population and industrial, tourism, and recreational developments. STAR is devoted to providing a better understanding of the physical features of arctic storms and their hazards, the processes controlling them, and our predictive capabilities for them. Furthermore, interactions with the local community,

including government and northern agencies, have been established so that the progress of STAR can be conveyed directly to these affected groups, and their guidance can be used in developing scientific plans.

STAR represents an opportunity to compare the structure of storms in different regions of Canada with different topographic forcings, such as those addressed by BASE, MAGS, and CASP. Comparisons to other international projects—such as Fronts and Atlantic Storm Track Experiment (FASTEX; Joly et al. 1999)—can also be made. However, STAR is not just addressing the physical features of storms; it is also focusing on the related hazards at the surface, weather prediction capabilities, and interacting effectively with local communities. Collectively, STAR is maximizing its benefits by building on the relevant scientific knowledge gained from other experiments.

Although STAR is not an International Polar Year (IPY) project, it is collaborating with Canadian and international IPY projects, such as The Observing System Research and Predictability Experiment (THORPEX) Arctic Weather and Environmental Prediction Initiative (TAWEPI), the Circumpolar Flaw Lead (CFL) System Study, the European IPY–THORPEX, and the Greenland Flow Distortion experiment (GFDex; Renfrew et al. 2008). For example, STAR modeling activities and developments are contributing to the development of the Canadian Polar Global Environmental Multiscale (GEM) model for future operational use—a key outcome of TAWEPI. In addition, a study of the effects of storms on sea ice is a collaborative initiative between STAR and CFL. Knowledge exchange relating to a variety of atmospheric issues will take place with international IPY projects through collaborative meetings and common symposia.

The objective of this article is to briefly describe the design and operation of the STAR project, data management issues, storms, and associated phenomena that were observed, and some results to date. Detailed accounts are available in the STAR Data Report (Fargey et al. 2008).

PROJECT OBJECTIVES. STAR is concerned with the documentation, better understanding, and prediction of meteorological and related hazards in the Arctic, including their modification by local topography and land–sea ice–ocean transitions, their effects on the local communities, and information that may lead to an assessment of hazard frequency relative to a changing climate. The overall objective of this 4-yr STAR network (2007–2010) is to better understand severe arctic storms and their associated hazardous conditions, and to contribute to their better prediction.

The majority of the enhanced detailed measurements were made in the vicinity of Iqaluit, Nunavut, although storms affecting other communities on southern Baffin Island were also of interest. Some enhanced measurements were also made at Pangnirtung.

The objectives are being realized through a focus on four themes:

1) Hazardous weather-related conditions in the Iqaluit area;
2) Regional hazardous weather-related conditions and sea ice effects;
3) Prediction capabilities and improvements; and
4) Interaction with the user community.

Three main hazards being investigated include:

1) Blizzards, blowing snow, and reduced visibility;
2) Storms producing snow and mixed-phase precipitation with significant accumulation; and
3) Storms, strong winds, and their effect on sea ice.

The primary motivation for STAR is the various forecasting and modeling issues that are evident in the Arctic, most of which are caused by storm–topography interactions and the seasonal variation of heterogeneous surface conditions (sea ice versus open water). Forecasting is made even more complicated by the data-sparse nature of the region's operational weather observing network. The following issues have been identified as challenges in forecasting and modeling high-impact weather in the Baffin region [Prairie and Arctic Storm Prediction Centre (PASPC) 2005, personal communication]:

1) *Winds.* Difficulties with wind speed and/or direction forecasts due to i) accounting for complex topography, leading to errors in the strength of topographically forced circulations, such as gap flow and barrier flows; and ii) incorrect advection of air masses associated with topographic effects.
2) *Timing of frontal passages.* Interaction of synoptic-scale systems and fronts with local topography and transitions from locally to synoptically forced flow. For models, this has to do with a resolution that captures neither the depth of the locally forced flow nor the interaction of the synoptic-scale system with the topography.

3) *Upslope precipitation.* Precipitation is a continuing challenge in the Arctic, and the operational Canadian regional model appears to have a systematic problem with capturing the intensity of precipitation associated with upslope flow; such events are common.
4) *Weather elements.* Hazardous weather conditions linked with low visibility, blowing snow, and aviation-related issues such as icing, ceiling height, and wind shear represent major prediction challenges. Although current models provide some guidance, the local influences (topography and ice/open water effects) create forecasting challenges, and many processes leading to these events remain to be studied in detail.

PROJECT AREA, CLIMATOLOGY, AND INSTRUMENTATION. *STAR Geography and Climatology.* STAR is geographically focused on the southern Baffin Island region of Nunavut, Canada. The area around Frobisher Bay on southern Baffin Island is dominated by two mountain ranges (Fig. 1). The Meta Incognita Peninsula, to the west-southwest, is characterized by low mountain ranges with a typical elevation of 600 m and peaks to about 750 m within 50 km of Iqaluit. On Hall Peninsula, to the north and northwest of Iqaluit, the mountains are generally higher, reaching about 1000 m within 100 km of the city, with a maximum elevation of 1295 m close to the southwest coast of Cumberland Sound. These mountains have a strong effect on the surface weather near coastal communities such as Iqaluit. The highest topography—elevations in excess of 2000 m—on southern Baffin Island is associated with the Penny Ice Cap on the Cumberland Peninsula north of Pangnirtung. Available operational meteorological data on southern Baffin Island are hourly surface observations at the locations shown in Fig. 1 and 12-hourly soundings at Iqaluit (63°45′N, 68°33′W).

In the southern Baffin Island region, the primary storm seasons are spring (March through May) and autumn to early winter (October through early December). The autumn season is the stormiest, when cold air from the north crosses relatively warm surfaces and warm air from southern latitudes. Snowstorms occur most frequently in autumn (October and November) and in winter (February). Freezing precipitation is relatively rare at Iqaluit compared to southern latitudes. Freezing precipitation occurs most frequently in spring (May) and autumn (October; Roberts and Stewart 2008). The wind direction most commonly associated with freezing precipitation in either season is from the southeast, although a secondary maximum of freezing precipitation occurs from the northwest.

Open water can exist in Davis and Hudson straits, even in midwinter, and can supply heat and moisture to the storms. The result is that storms can reintensify in autumn and winter, but this area is also considered a "burial ground" for intense storms during all seasons (e.g., Hudson et al. 2001).

Local topographic effects from the Meta Incognita and Hall Peninsulas to the south and north of Frobisher Bay, respectively (see Fig. 1), are evident in the Iqaluit wind climatology (Fig. 2). Wind speeds in excess of 60 km h^{-1} occur almost exclusively from the northwest and southeast. With the annual shifting of the polar front and preferred storm tracks, there is a change in prevailing wind direction at Iqaluit from the northwest in winter to the southeast in summer. Because of channelling effects, northwesterly surface winds at the Iqaluit airport may be stronger and from a different direction than over the higher terrain in the interior of the island. Strong northeasterly winds over the interior are often deflected to the northwest.

Topographic effects can also result in high wind speed (gap and barrier flows) and significant precipitation events (e.g., Martin and Moore 2005; Nawri

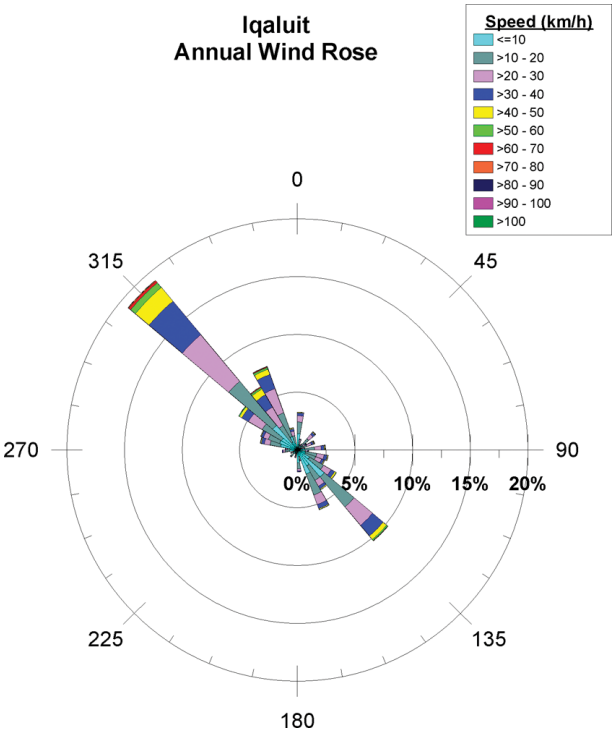

Fig. 2. Iqaluit annual wind rose valid between 1960 and 2003. The color legend provides wind speed ranges. A clear wind direction bias (northwest–southeast) is evident as a result of surrounding topographic effects.

and Stewart 2006, 2008). Occasionally, strong northeasterlies may reach the surface in Iqaluit, or they may generate intense horizontal vortices (rotors) at the sharp rise of the terrain (e.g., Ozawa et al. 1998; Hudson et al. 2001). Although no serious aviation accidents have occurred in Iqaluit, this shear is a potential hazard to aircraft (Mahapatra and Zrnic 1991; Kaplan et al. 2000), and it has been reported on numerous occasions by pilots of various airlines (Environment Canada 2006, personal communication). The highest observed 10-m wind speed at Iqaluit Airport prior to the record-breaking event in 2007 (mentioned in the introduction) was 129 km h^{-1}. Climatologically, wind speeds above 90 km h^{-1} occur fewer than once a year, in either autumn or winter. However, strong low-level jets with hourly wind speeds greater than 60 km h^{-1} are reported about 25 times a year on average, mainly from autumn to spring and primarily from the northwest (Nawri and Stewart 2006, 2008).

The blowing snow/blizzard season in Iqaluit extends from October to May and peaks in January and February (an average of 80–90 h of blowing snow reports per month). Most January and February events with more extreme visibility reductions (to ≤3 mi or 4.8 km) occur with cold temperatures (<–25°C), and visibilities less than 0.8 km (or 1/2 mi) occur one-quarter of the time during events with visibilities ≤4.8 km. Annually, 90% of winds from the northwest to the east with speeds exceeding 60 km h^{-1} are associated with blowing snow. The most extreme visibility-restricted events (≤0.8 km) occur from the northwest 95% of the time.

The average sea ice freeze-up dates in and around southern Baffin Island (e.g., Frobisher Bay) are from middle to late November. Break-up dates occur in early to mid-July, and there is typically no ice in the summer (except for the unusual iceberg). Strong wind events can have major effects on coastal sea ice and can create open water areas that provide moisture for the formation of low cloud and fog. During autumn and early winter, the cloud and fog are often composed of supercooled water, and they are capable of producing both freezing drizzle and significant aircraft icing.

Within our study area, there is evidence that reductions in sea ice concentrations are strongest during the shoulder seasons, when the ice is in retreat or expanding (Moore 2006). For example, passive microwave data analysis (Cavalieri et al. 2008) performed between 1979–2008 by several of the STAR authors shows that sea ice extent (SIE; expressed as a percentage of the total basin area, with a minimum of 15%) in late October in Foxe Basin has decreased by 23% $decade^{-1}$. In addition, the trend in SIE is –27% $decade^{-1}$ between late October and early November in Hudson Strait, –10.9% $decade^{-1}$ during November in Davis Strait, and –24% $decade^{-1}$ in the Labrador Sea. All trends are >99% statistical confidence.

The STAR period experienced a "normal" fast ice freeze-up/consolidation in late November within Frobisher Bay; however, the surrounding regions of Hudson Strait and Davis Strait had below-average ice concentrations. It is unclear whether the ice reductions are indicative of a secular trend associated with anthropogenic climate change (Serreze et al. 2000), the result of low-frequency variability in the climate system (Deser et al. 2000; Morison et al. 2000), or with changes farther north in Baffin Bay and the Gulf of Boothia—the source region for sea ice that is advected into the region (Prinsenberg 1986; Barber et al. 2001). Such a trend, regardless of its origin, will affect the weather systems in the region through an increase in the exchange of energy from the ocean to the atmosphere. GCM simulations suggest that there may be an increase in cyclogenesis and wind speeds in the region in the coming years (Knippertz et al. 2000).

STAR instrumentation. Arctic storms and severe weather were sampled using standard meteorological field measurements and remote sensing. Measurements were collected during two campaigns in autumn 2007 (10 October–30 November) and winter 2008 (primarily 1–29 February). The base for surface observations was the Environment Canada office in Iqaluit. Meteorological instruments were installed in the last week of September and remained operational throughout the autumn field campaign. Certain instrumentation remained in the field for both the autumn storm and winter blowing snow projects.

NRC RESEARCH AIRCRAFT. The National Research Council of Canada's Convair-580 research aircraft was instrumented by Environment Canada and NRC to collect internal storm measurements of cloud microphysics, thermodynamics, wind, and the 4D dynamic and precipitation structures of storms within a 500-km radius of Iqaluit from 5 to 30 November 2007. The aircraft enabled STAR scientists to probe storms as they approached the region as well as during their passage through and departure from the study area. The aircraft also provided sensor validation flights for Cloudsat overpasses in the Arctic. A list of all aircraft instrumentation appears in Table 1.

Three radars were onboard to provide remotely sensed measurements of clouds and precipitation:

Table 1. NRC and Environment Canada Convair-580 research aircraft instrumentation list for STAR. Total water content (TWC); Rosemount Icing (RICE); National Center for Atmospheric Research (NCAR); Droplet Measurement Technologies (DMT); Commonwealth Scientific and Industrial Research Organisation (CSIRO); counterflow virtual impactor (CVI); Cloud Aerosol and Precipitation Spectrometer (CAPS); Temperature (T); Stratton Park Engineering Company (SPEC) Inc.; Cloud Particle Imager (CPI); infrared thermometer (IRT).

NRC Convair—580 and EC aircraft instrumentation	Measurement
Atmospheric state	
Rosemont 102 probe × 3	Temperature
NCAR reverse flow probe	Temperature
LI-COR LIC2G2 water vapor/CO_2 instrument	H_2O mixing ratio, CO_2 mixing ratio
EG7G chilled-mirror hygrometer	Humidity
Rosemount 858 gust probe	Vertical velocity
CR-2 water vapor measurement system	Humidity, low vapor concentrations
LWC and TWC	
RICE probe	Detects supercooled water
Vibrameter	Detects supercooled LWC
Nevzorov LWC/TWC probe	Separate estimates of LWC and TWC
PMS CSIRO King Probe	LWC
Cloud microphysics	
DMT CVI for TWC	TWC
DMT CAPS	T, LWC cloud size distribution (0.5–1500 μm)
SPEC CPI	Cloud particle images (15–2500 μm)
PMS FSSP-100X	Small particle spectrum (3–45 μm)
PMS FSSP-100X	Small particle spectrum (5–95 μm)
PMS FSSP-002	Small particle spectrum (3–45 μm); without sample tube
PMS 2D2C	Cloud particle images and spectra, nominally 25–800 μm
SPEC 2DS (10-μm configuration)	Cloud images and spectra 10–1280 μm, orthogonal channels
PMS 2DP	Cloud particles images and spectra, nominally 200–6400 μm
PMS 2DC grey	Grayscale images of cloud particles, nominally 15–960 μm
Radiometers	
Heitronics KT19.85 IRT	Cloud emissivity, surface temperature; nadir view; narrow field of view
Kipp and Zonen broadband visible radiometers	Broadband hemispheric visible radiation; zenith and nadir view; 305–2800 μm
Epply broadband pyrgeometers	Broadband hemispheric infrared fluxes; zenith and nadir view; 3.5–50 μm
ProSensing upward-looking G-band radiometer	Multichannel centered on 183.31 GHZ; derived parameters water vapor and liquid water paths above aircraft
Other remote sensing	
Ka-band upward- and downward-looking radar	Radar cross sections (reflectivity only)
NAWX X-band/W-band radar, dual polarization, Doppler, upward/downward/sideways looking	Radar cross sections and looking sideways; Z/Doppler fields

Ka-band (8.7-mm wavelength) upward-/downward-looking radar providing reflectivity, and the NRC Airborne W-band (3.2-mm wavelength) and X-band (3.2-cm wavelength; NAWX) polarimetric Doppler radar (upward/downward/sideways looking) providing reflectivity, polarimetric characteristics, and

Doppler velocities. The W-band radar is essentially a "cloud" radar, capable of detecting cloud droplets and ice crystals; precipitation-sized particles are not required to be present within the cloud to obtain useful measurements, unlike standard surface-based weather radars. The X-band radar is generally less sensitive to cloud than the other radars, depending on hardware, operating configuration, and processing capabilities. The combination of all radars provides an excellent way to study cloud dynamics and their microphysical structure as well as precipitation mapping (rates, location) and microphysics (sizes, composition) by looking at reflectivities, dual/triple frequency ratios, polarization, and Doppler velocities as well as dual and triple frequency reflectivity all at the same time. (More information about the NAWX radar can be found at www.nawx.nrc.gc.ca/nawx.html.)

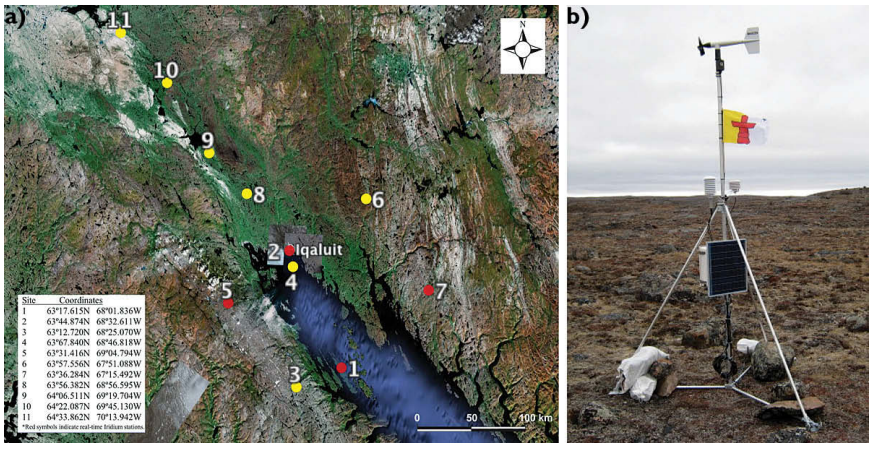

Fig. 3. (a) STAR mesonet of surface weather stations. Red markers indicate stations with real-time data access via Iridium satellite phone. (b) Example of the remote mesonet weather stations. The official Nunavut Territory flag was mounted on each station.

The NRC aircraft flew approximately 48 hours during the project. This time was divided between 14 missions with variable objectives, with a total of 56 dropsondes being deployed during nine aircraft flights (Table 2). The first flight was into the remnants of Hurricane Noel, which was the most severe hurricane of 2007 in terms of Caribbean casualties (>150; NOAA 2007). In contrast, the final flight had a very local focus, sampling the cloud system directly over Iqaluit for remote sensing validation purposes. Additional flights took the research aircraft into Foxe Basin, Hudson Strait, Ungava Bay, Davis Strait, and Cumberland Sound, and locally in Frobisher Bay (see Fig. 1).

Upper-air observations. Iqaluit is the only location on southern Baffin Island where regular 12-hourly upper-air observations are made. During storms and other appealing weather events, the standard upper-air releases were supplemented with additional radiosondes at 3- or 6-hourly intervals. All radiosondes were Vaisala RS92. From the period of 10 October–30 November 2007, there were 51 special radiosonde releases made by the STAR project.

A portable radiosonde unit was deployed in the community of Pangnirtung to conduct simultaneous launches with those in Iqaluit during selected severe weather events (using Vaisala RS92). A total of 18 radiosondes were released in Pangnirtung between the dates of 2 and 18 November 2007.

Surface-based remote sensing observations. A portable X-band Doppler radar was deployed at the Environment Canada office in Iqaluit (10 October–30 November 2007). No operational radars exist in northern Canada. This instrument was used in real time to map precipitation and wind fields within a radius of approximately 50 km of Iqaluit. It was also used to validate satellite- (e.g., Cloudsat) and surface-based precipitation measurements. The radar was run in a series of four scan modes—plan position indicator (PPI), volume scans, RHI, and vertical stare—with one full cycle repeated every 15 minutes.

A passive microwave radiometer (Radiometrics WVR-1100) provided time series measurements of column-integrated water vapor and liquid water content over Iqaluit. The STAR radiometer operated looking upward, at a sampling resolution of about 1 minute, from 10 October to 30 November 2007.

An acoustic Doppler sodar system (Remtech PA1-NT) was also used at Iqaluit to assess three component winds from 0 to 1.2 km AGL, with a 30-m vertical resolution, every 30 minutes during 10 October–30 November 2007.

Weather station mesonet. A small mesonet of 10 automatic weather stations was deployed within a 100-km radius of Iqaluit because of the dearth of operational data in the study area (Fig. 3). Nine of

Table 2. Summary of the IOPs during STAR. YFB is Iqaluit and XVP is Pangnirtung. The "No. YFB sondes" column shows the total number of "special" radiosondes (those released outside of 1200 and 0000 UTC) released in Iqaluit as well as the total number released in Pangnirtung (in parentheses). "Yes" in the "aircraft flight" column means that an aircraft mission took place for that IOP; notice that sometimes multiple flights occurred (in parentheses). The number in the "No. dropsondes" column refers to the total number of dropsondes for each IOP. The last column states the purpose of the IOP with a brief description.

IOP	Start (UTC)	End (UTC)	No. YFB sondes	Aircraft flight	No. dropsondes	Mission purpose
1	2100 15 Oct	1800 17 Oct	8			Low near south Baffin Island with significant snowfall (6–8 cm) in YFB
2	1800 20 Oct	0000 21 Oct	2			Low in north Quebec with orographic snowfall on south Baffin Island; upper flow regimes sampled
3	0600 26 Oct	0600 27 Oct	7			Low passing just south of Iqaluit; northern edge of system sampled
4	1200 29 Oct	1800 30 Oct	3			Low-level trough moved through south Baffin; 3 cm of snow in YFB and strong winds behind system
5	1200 3 Nov	1200 4 Nov	4 (2 in XVP)			Upper trough with snow and strong winds in YFB and XVP
6	1600 5 Nov	0000 6 Nov	7 (4 in XVP)	Yes	4	Remnants of Noel with moderate winds in YFB and XVP; aircraft into Noel
7	0000 6 Nov	0000 7 Nov	1	Yes		Aircraft Cloudsat pass over Iqaluit with mesoscale convergence and snow in YFB
8	2100 7 Nov	0700 8 Nov	3	Yes	13	Low to south of Baffin, with upslope precipitation on south shores and weaker snow in YFB; aircraft for upslope processes
9	2100 9 Nov	0200 10 Nov	1	Yes	6	Convection over Hudson Strait. Upslope snow on west coast of Baffin and unexpected snowfall in YFB; aircraft sampled convection and upslope processes
10	2100 11 Nov	1600 12 Nov	5	Yes	6	Short-wave trough with snow in YFB/XVP and significant upslope in Cumberland Sound (aircraft)
11	1900 16 Nov	0000 19 Nov	23 (12 at XVP)	Yes (3 flights)	16	Most intense storm during STAR, with significant snow in YFB and some in XVP; aircraft used for warm front, low center, mesoscale convergence, and two Cloudsat missions
12	1530 20 Nov	2230 20 Nov		Yes (2 flights)		Aircraft mission for Cloudsat and convergence with snow near Ungava Bay
13	1600 22 Nov	1900 22 Nov		Yes		Aircraft Cloudsat mission over Hudson Strait
14	1600 23 Nov	2000 23 Nov		Yes	4	Aircraft Cloudsat misson into Foxe Basin upper low
15	1500 28 Nov	1830 28 Nov		Yes	5	Aircraft Cloudsat mission near Cumberland Sound with low cloud
16	1900 28 Nov	0000 29 Nov	3	Yes	1	Weak low tracked over south Baffin with light snow in YFB; aircraft sampled low and upslope precipitation

these stations (all except station 2) measured 3-m wind velocity, pressure, 2-m temperature, and 2-m humidity every 10 minutes. The weather stations were positioned over various forms of topography, in consultation with Environment Canada forecasters, to assess storm influences on surface weather. Through collaborations with local northern groups, Indian and Northern Affairs Canada (INAC), and Qulliq

Energy Corporation, four of the stations (indicated in red on Fig. 3) provided near-real-time data (once a day) by iridium modem. One of the 10 stations was a standard 10-m tower at the Environment Canada site in Iqaluit (station 2 in Fig. 3). This tower was equipped with similar instrumentation as the other stations, but it also had anemometers at stations 10, 4, 3, 2, and 1, two Sentry visibility sensors, and vertical temperature gradient measurements. In addition to the 10 stations, two automatic weather stations were deployed: one in Pangnirtung (not shown in Fig. 3), from 13 October to 18 November 2007; and another on the fast ice in Frobisher Bay (station 4 in Fig. 3). The latter station was collocated with an ice motion GPS buoy once ice conditions permitted (December 2007–May 2008). Besides air temperature, humidity, and wind sensors, the fast ice station was outfitted with thermocouples to profile the snow and ice, and upwelling shortwave and longwave radiation.

The mesonet weather stations were operational during both autumn and winter field campaigns and were dismantled by mid-April 2008, except for the four real-time stations and the fast ice station. As part of STAR's commitment to long-term research and support for northern communities, the four real-time stations have been left for INAC and Qulliq Energy for their continued use.

Special surface observations. Special instruments set up at the Iqaluit Environment Canada office site augmented other instrumentation. Historically, accurate precipitation measurements during storm events in the Arctic are difficult to acquire because of strong winds that can cause the underestimation of precipitation measurements by up to 100% if not accounted for (e.g., Goodison 1978; Goodison and Yang 1995; Goodison et al. 1998). To minimize this problem, STAR collaborated with Environment Canada to construct a double-fence facility with a Genore snow measurement system (e.g. Smith 2008). This system has been used by Environment Canada for several years in other Canadian locations. In conjunction with gauge precipitation measurements, a Thies Clima laser precipitation sensor was used for providing 1-min averaged precipitation type, size distribution, and fall velocity. Further analysis of precipitation was conducted using a high-resolution digital microphotography camera.

The fast ice weather and ice station provided information on the geophysical and thermodynamic state of the snow-covered sea ice throughout the winter and spring periods. The site was visited by students of Nunavut Arctic College and the Nunavut Research Institute to check the integrity of the station and collect data on snow thickness, density, and grain size as well as time series records of ice thickness. These data are being used to examine how storms affect the integrity of land-fast first-year sea ice.

During the February winter program, several instruments were used at the Iqaluit Environment Canada site in association with the 10-m tower and visibility instrumentation, to focus primarily on blowing snow events. Blowing snow particle counters were deployed, which count particles as they pass between a light source and a detector (e.g., Brown and Pomeroy 1989; Gordon and Taylor 2009a). A camera system used a similar method to also measure the size distribution of blowing snow particles. An electric field mill was used to measure the strength of the electric field generated by the electrostatic charging of blowing snow particles. Blowing snow mass flux was measured using an array of snow traps, and density measurements of the snow surface were made throughout the study. Many of these measurements have been made in other regions of Canada; hence, further details of these techniques can be found elsewhere (e.g., Savelyev et al. 2006; Huang et al. 2008; Gordon et al. 2009; Gordon and Taylor 2009b). The "Storm cases and selected results" section provides examples of current blowing snow research.

ATMOSPHERIC MODELING. Along with the Canadian operational GEM 15-km horizontal-resolution model run by Environment Canada, STAR used the nonhydrostatic 2.5-km horizontal-resolution limited-area version of the GEM model (GEM-LAM), run in real time over the STAR domain once a day. The GEM-LAM domain and its topography are depicted in Fig. 1. The University of Toronto also made real-time fifth-generation Pennsylvania State University–National Center for Atmospheric Research Mesoscale Model (MM5, version 5) forecast model products available online each day over a similar domain as GEM-LAM. Standard model output fields were provided over the limited domain and along specialized cross sections through Iqaluit: along and perpendicular to the terrain, along Cumberland Sound, and where required for flight planning.

Comparisons between GEM and GEM-LAM over the south Baffin region show that many of the model forecast differences are a result of the different model resolutions in this region of highly variable terrain and strong topographical forcing. For example, the GEM-LAM eastern domain experiences more precipitation, reflecting moisture-laden systems moving northward from the Labrador Sea, with a peak of

precipitation over the mountainous east coast, as a result of upslope flow. The red contour in Fig. 4a shows where GEM-LAM, on average, produced >30% more precipitation than the GEM, predominantly over the mountainous Cumberland Peninsula where topographic effects are largest. Over the western domain, GEM persistently produced large areas of very light precipitation to a much greater extent than did GEM-LAM, as shown by the white contour in Fig. 4a (where GEM produced, on average, >30% more precipitation than GEM-LAM). Work is ongoing to explain these differences.

Figure 4b shows the average wind speed for GEM-LAM at 1800 UTC for cases where the winds were at least 5 m s^{-1} (or ~ 10 kt). When both GEM and GEM-LAM predicted winds ≥5 m s^{-1}, it was rare for GEM winds to be stronger than those of GEM-LAM. The red contours in Fig. 4b show where GEM-LAM winds, on average, exceeded the GEM winds by at least 2 m s^{-1} (~ 4 kt; this value was selected arbitrarily, for illustration purposes). The red contoured areas are very much tied to topographical influences along the complex coastlines and over higher terrain.

Both GEM-LAM and MM5 are also being used for postanalysis case studies. Some examples are provided in the "Storm cases and selected results" section. Where possible, special STAR datasets—including upper-air, mesonet, aircraft, and radar data—will be ingested in data assimilation experiments as part of future analysis.

Besides looking at short-term weather events, one STAR project is focusing on future changes in strong wind and high-precipitation events in the southeast Arctic, using regional climate models (RCMs). By studying synoptic conditions from historic extreme wind and precipitation events, including those during STAR, these flow patterns can be used to assess RCM hindcasts and future transient simulations of these events under various greenhouse gas scenarios.

REAL-TIME DECISIONS AND FORECASTS.

The STAR weather/logistics office was located at the Iqaluit Environment Canada facility—the same location as the specialized equipment, portable radar, and upper-air site. It had four main purposes: to make decisions on project operations, to communicate these decisions to participants, to archive data and coordinate rudimentary analysis during the project, and to maintain a log of activities.

Logistics and flight planning meetings took place twice daily: once in the morning (usually 1000 EDT) to coordinate the day's activities and another in the evening (typically 1900–2000 EDT) to discuss the next day's expected activities. Meeting times were adjusted and supplemented depending on storm events, flight times, and flight duration. From 10 October to 1 November 2007, a virtual weather office was employed using Web-/telephone-based weather briefings performed by an operational meteorologist from Environment Canada in Edmonton, usually twice per day, when new model products were available. From 2 to 15 November 2007, three meteorologists from Environment Canada were present at the STAR field office, providing twice-daily weather briefings.

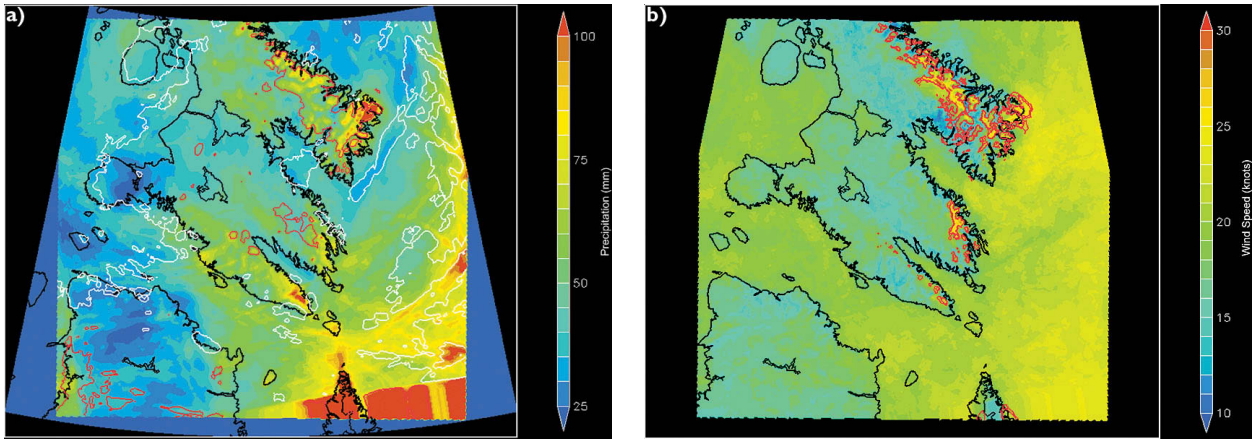

Fig. 4. (a) Mean daily precipitation amounts (mm; water equivalent, shaded) from the GEM-LAM between 10 Oct and 5 Dec 2007. Data at the extreme southeastern-most part of the figure (orange-red colored "triangular" piece) are invalid. The red contour indicates where the GEM-LAM, on average, produced >30% more precipitation than the GEM. The white contour shows where GEM produced, on average, >30% more precipitation than GEM-LAM. (b) The mean wind speed (kt; shaded) for GEM-LAM at 1800 UTC for cases where the winds were at least 5 m s^{-1} (~10 kt). The red contours show where GEM-LAM winds, on average, exceeded the GEM winds by at least 2 m s^{-1} (~4 kt).

The types of data that were available for forecast support included the regular operational data and the specialized GEM-LAM and MM5 outputs. Some additional data (e.g., polar-orbiting satellite and specialized model output) were sent to a central server that made the data accessible to the STAR group in real time and were then archived for the project.

STORM CASES AND SELECTED RESULTS. Sixteen intensive observation periods (IOPs) took place between 10 October and 30 November 2007. Table 2 identifies the start and end dates and times, the number of special radiosonde releases (not including the regular operational releases), applicable aircraft flights, and dropsondes as well as the purpose of each IOP. Multiple purposes and types of phenomena may have been sampled for any given IOP. The table shows that a wide variety of weather/phenomena was observed during STAR, with two IOPs having multiple aircraft flights. Six closed-surface low pressure systems crossed southern Baffin Island during this period, with two of them being major systems (central surface pressures <990 hPa).

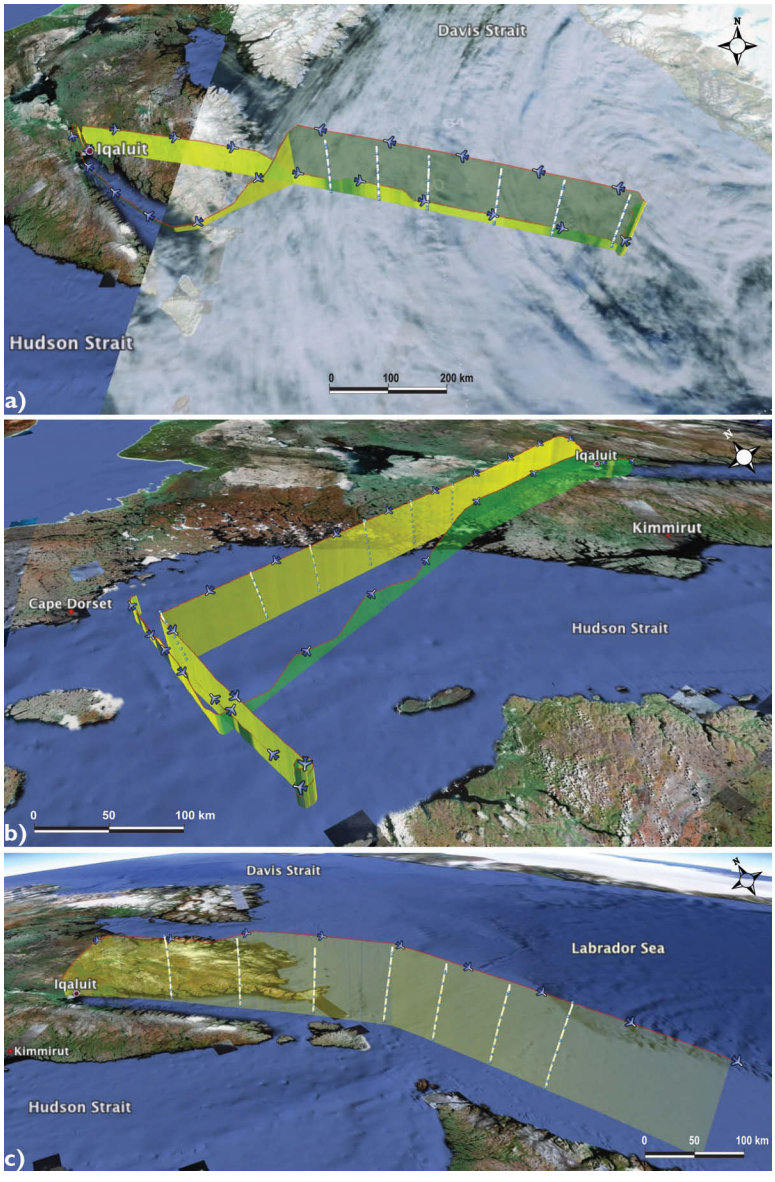

Fig. 5. (a) Flight track and overlain 1630 UTC MODIS satellite image of IOP6 1355–1815 UTC 5 Nov (remnants of Hurricane Noel). The aircraft heading is shown by the aircraft icon. The locations of the dropsondes are indicated in white. (b) Same as (a) but for IOP11 1145–1920 UTC 17 Nov. (c) Same as (a) but for IOP9 2130 UTC 9 Nov–0125 UTC 10 Nov.

The analysis of STAR data is well underway. A few examples of this effort are discussed next.

IOP6 (5–6 November 2007). This was a significant storm, sampled solely by aircraft and tracked from eastern Canada into the Davis Strait through to Greenland on 5–6 November 2007. It was the remnants of Hurricane Noel, the most severe hurricane in 2007 in terms of tropical region casualties. The hurricane initiated off of the coast of Africa on 16 October 2007, intensified into a hurricane in the Bahamas (maximum intensity category 1), and maintained hurricane force winds over the eastern United States and Canada as an extratropical storm. The storm continued to track northward, into Davis Strait from 4 to 5 November 2007, as a powerful high-latitude system (central pressures near 965 hPa). An MM5 modeling study is ongoing on the extratropical transition of Noel as well as its evolution within the STAR domain.

Figure 5a shows the STAR flight track into the storm system. The STAR team sampled the storm's northeastern edge, flying at low altitudes (400 m–1 km MSL) inbound and higher altitudes (5 km MSL) outbound, with multiple dropsondes, W-, X- and Ka-band radar coverage and cloud microphysical measurements. Minimum equivalent sea level pressure and maximum wind speeds measured at low levels were

~967 hPa and >24 m s^{-1} (or >85 km h^{-1}), respectively. An example of the aircraft upward-/downward-looking W-band radar reflectivity field is shown in Fig. 6, as the aircraft was inbound to the storm at low altitudes. Cloud tops ranged between 5.5 and 6.5 km MSL, with lower and more defined cloud tops closer to the low center, based on flight notes (see also Fig. 6). Cloud-base heights were typically near 500 m through most of the low-level flight, with little to no turbulence, based on visual observations. Most of the precipitation was generated at or below 3 km MSL, with considerable organization, embedded higher "cores" of precipitation, and large gradients of reflectivity (see Fig. 6)—all features of banded-like structures as seen on the Moderate Resolution Imaging Spectroradiometer (MODIS) satellite image in Fig. 5a.

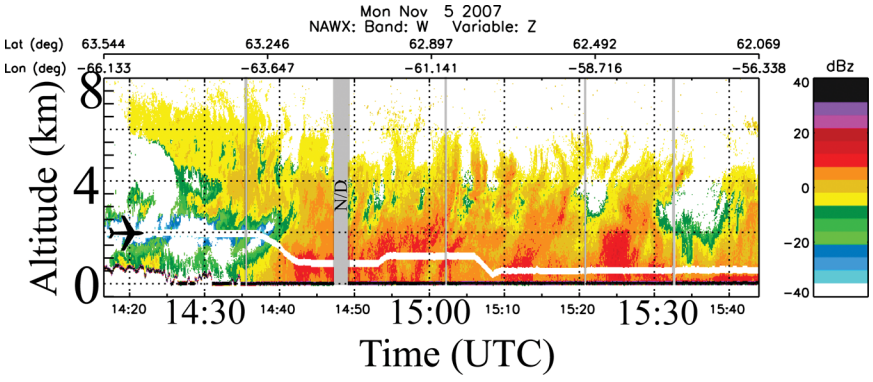

Fig. 6. W-band aircraft upward-/downward-looking radar reflectivity during part of the inbound (toward the storm) leg of IOP6 between 1415 and 1545 UTC 5 Nov 2007. The solid white line denotes the aircraft altitude above sea level (*y* axis). The bottom *x* axis is time in UTC and the top axis is latitude/longitude. The gray shading signifies no data (N/D).

MM5 simulations of the storm showed relatively good agreement with low-level flight data, aircraft radar precipitation mappings, and cross-sectional analysis from dropsondes (Fig. 7), although the observed low-level jet was closer to the surface than indicated by the model, and the observed warm-core thermal structure was slightly warmer than indicated by the model. MM5-modeled surface winds were consistently and significantly weaker than observations as Noel made its extratropical transition (not shown). The warm core, by deepening the low pressure at the surface, is most likely responsible for the intensification of surface winds (Rasmussen et al. 1993). Modeling and observational analysis also suggest that the high-latitude system reintensification was primarily caused by midlevel dynamic forcing from an upper-level trough as potential vorticity was transferred downward from the upper troposphere. The Eliassen–Palm flux diagnosis in cylindrical isentropic coordinates indicates in this case that as the cyclone intensifies, the upper-level eddy momentum forcing is more important than the upper-level eddy heat forcing.

IOP11 (17–19 November 2007). IOP11 contained the most intense storm that affected the southern Baffin Island region during STAR, with the lowest central pressures (near 964 hPa) and a total of 8 mm of snow water equivalent measured in Iqaluit. Three research flights were devoted to IOP11, with dropsondes in the first flight released through the warm front (see Fig. 5b) containing a rain/snow boundary, as the low center was located in central Quebec. During the first flight, the Convair was grounded in Goose Bay, Labrador, overnight because of poor airport conditions caused by widespread hazardous weather in the southern Baffin Island region. The two remaining flights sampled cloud and precipitation in the wake of the storm and in the low center, including two Cloudsat pass validation opportunities (not shown).

Cross-sectional analysis of data from the dropsondes and aircraft radar from the first flight reveals part of the thermal and precipitation structures of the warm front (Fig. 8). The lower frontal boundary is clearly marked by 1) the wind shears at the lower frontal boundary (thick dashed line in Fig. 8a represents the upper bound of the easterly flow ahead of the warm front), with winds above the dashed line sharply veering to a southerly flow above this; 2) low-level jet (>20 m s^{-1}) at 500 m MSL and midlevel jet (near 1235 UTC) at ~3 km MSL beneath the warm nose; and 3) the location of the lower and upper boundary of the overriding warm air. Frontogenesis was also occurring during the release of the dropsondes (not shown). The W-band radar vertical cross section of reflectivity from takeoff in Iqaluit to the heavy precipitation area shows a notable stronger reflectivity below 4 km between 1210 and 1235 UTC (Fig. 8b). There is no indication of a melting layer; hence, cloud moisture (possibly) consisted of mostly ice crystals with possible aggregation between 2 and 3 km MSL. Starting around 1245 UTC, all three radars (only W-band

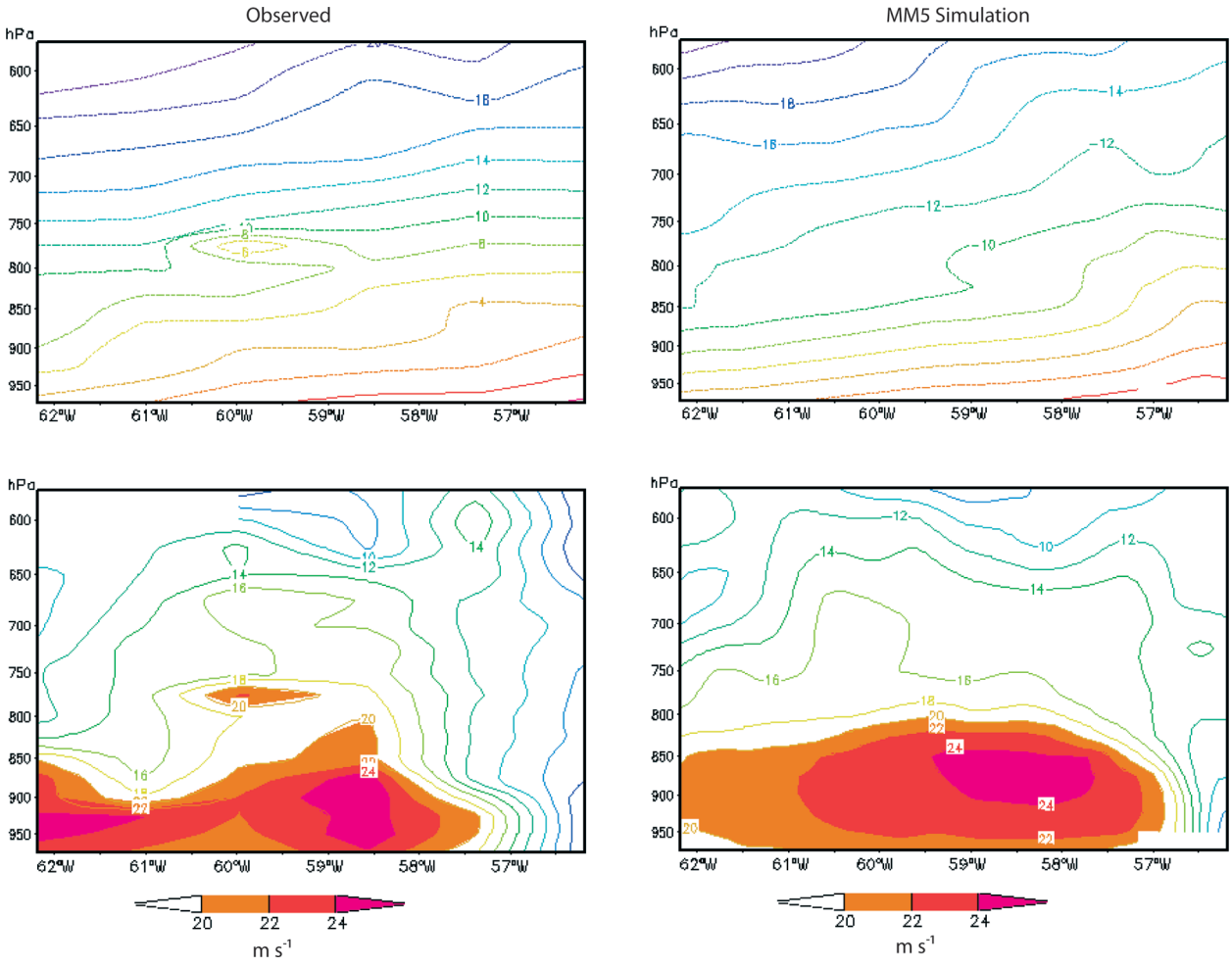

Fig. 7. (left) Dropsonde and (right) MM5-modeled vertical cross sections of (top) temperature and (bottom) wind speed. The *y* axis is sea level pressure and the *x* axis is longitude west. Wind speeds ≥20 m s^{-1} are shaded. Model output is valid for 1700 UTC 5 Nov 2007, within the period of the dropsondes.

data shown in Fig. 8b) started to show a well-defined bright band at around 2 km MSL, in agreement with Fig. 8a. It can be seen from the figure that there is an appreciable amount of attenuation in the W-band signal in the rain region (below 2 km). The overall warm-front structure is very similar to that of other mid- and high-latitude warm fronts (e.g., Hanesiak and Stewart 1995; Hanesiak et al. 1996); however, the mixed precipitation area in IOP11 was much less significant than in some midlatitude counterparts, for reasons yet unknown. Analysis is ongoing, using other aircraft data to characterize the microphysical structure of the front and other more detailed kinematic and thermodynamic characteristics as well as GEM-LAM model analysis and validation.

As the warm front and surface low tracked over southern Baffin Island, producing precipitation in Iqaluit, the most intense radar reflectivity (as measured by the surface radar deployed in Iqaluit) reaching the surface occurred near 0000 UTC on 18 November (Fig. 9a). As was observed in other events at Iqaluit, this event had an increase in reflectivity aloft (at approximately 1200 UTC 17 November) and had periods when the radar reflectivity did not reach the surface (i.e., virga). The maximum height of the radar echo did not occur near the start of the event but rather at a considerably greater height (7 km) above the radar once the low center made its way over Iqaluit. Similar results were found in the western Canadian Arctic (Hudak et al. 2004), where at times radar reflectivities decreased toward the surface, and cloud top heights were found to be similar to the observations in this STAR case (IOP11). Several cloud layers sometimes occurred during the frontal passage (see Fig. 9a). In fact, one particular event (not shown) had as many as five cloud layers, indicating complex meteorological structures. Stewart et al. (2004) also found many cloud layers present during

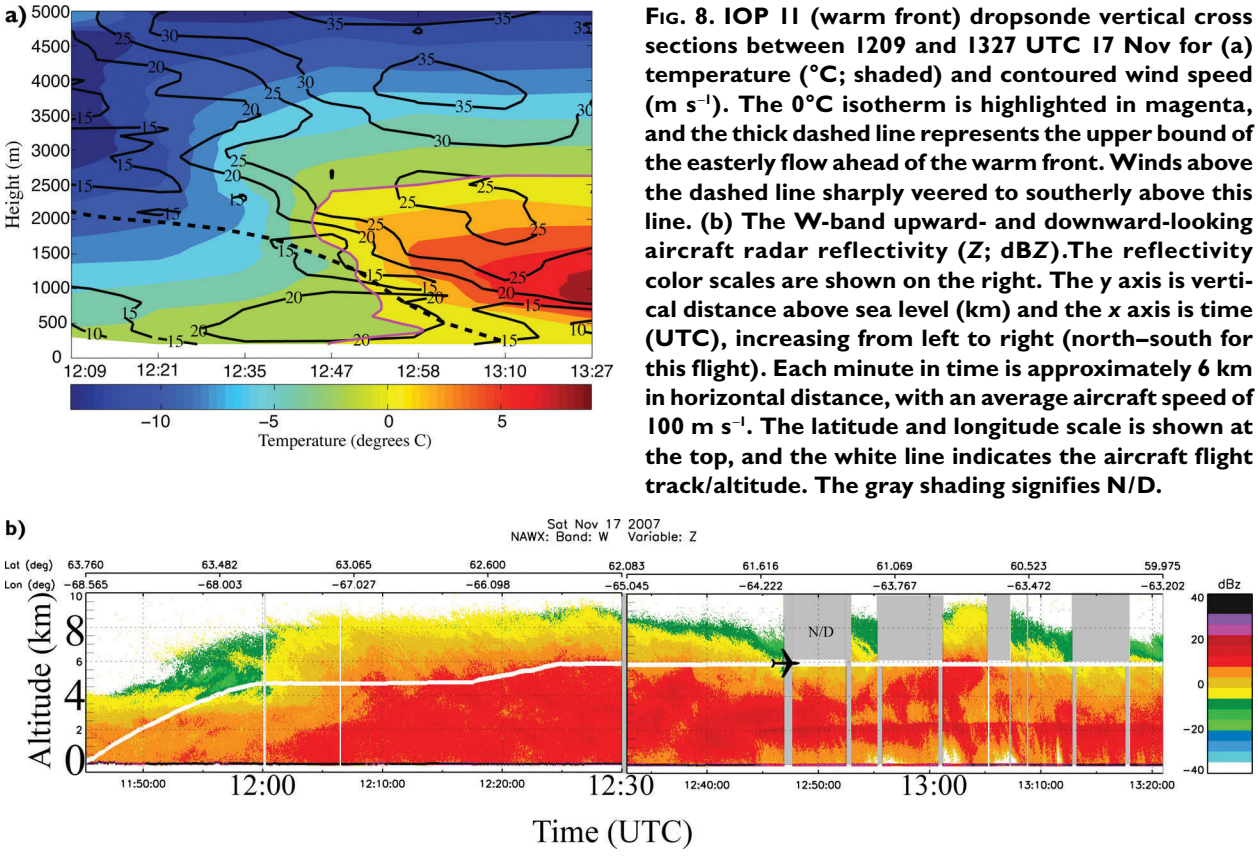

Fig. 8. IOP 11 (warm front) dropsonde vertical cross sections between 1209 and 1327 UTC 17 Nov for (a) temperature (°C; shaded) and contoured wind speed (m s^{-1}). The 0°C isotherm is highlighted in magenta, and the thick dashed line represents the upper bound of the easterly flow ahead of the warm front. Winds above the dashed line sharply veered to southerly above this line. (b) The W-band upward- and downward-looking aircraft radar reflectivity (*Z*; dBZ).The reflectivity color scales are shown on the right. The *y* axis is vertical distance above sea level (km) and the *x* axis is time (UTC), increasing from left to right (north–south for this flight). Each minute in time is approximately 6 km in horizontal distance, with an average aircraft speed of 100 m s^{-1}. The latitude and longitude scale is shown at the top, and the white line indicates the aircraft flight track/altitude. The gray shading signifies N/D.

precipitation events in the western Canadian Arctic, at times as many as five.

The normalized contoured frequency by altitude diagrams (CFADs) for the fall speeds of precipitation during 17–19 November 2007 can be seen in Fig. 9b. Similarities between this event and all other precipitation events observed during STAR include a fall speed of 1 m s^{-1} near the surface and an increase in vertical velocity of the hydrometeors as they fall toward the surface, implying that there is deposition and/or aggregation aloft. Differences include the altitude at which the increase in fall speed occurs (Fig. 9b). The increase in fall speed suggests that the hydrometeors increase in size at various altitudes within the cloud, depending on microphysical processes, which is similar to findings in other Canadian east coast weather systems (e.g., Stewart 1991).

IOP9 (9–10 November 2007). A low-level convection and roll vortices case was sampled using aircraft over Hudson Strait (see Fig. 5c for the flight track), allowing for observations never before available in this part of the Arctic. This system produced unexpected and highly rimed accumulations of snow (2–3 cm) in Iqaluit between 1900 UTC 9 November and 0200 UTC 10 November. One special radiosonde was released in Iqaluit at 2100 UTC 9 November to sample the thermodynamic state of the atmosphere during the event, and special precipitation microphotographs were taken. Aircraft W-band radar highlights the structure of the convective cells, with cloud tops between 2 and 2.2 km, and individual cells ranging between 5 and 8 km in width (Fig. 10), similar to other high-latitude observations (e.g., Renfrew and Moore 1999). Distances between the cells perpendicular to the mean flow were 5–8 km and about 5–6 times this distance parallel to the mean wind flow, comparable to other studies (Atkinson and Zhang 1996; Renfrew and Moore 1999). Some of the convective cells have significant updraft cores (blue shades up to 5 m s^{-1} in Fig. 10b), ≤2 km in horizontal extent that suspended precipitation aloft. GEM-LAM model soundings prior to the event were suggesting surface-based convective available potential energy (SBCAPE) from 150 to 200 J kg^{-1}, depending on the surface temperature selected. The SBCAPE predicts maximum updrafts between 17 and 20 m s^{-1}, significantly larger than those observed. Moderate turbulence and light icing were observed during the flight when flying within the cells (not shown). Cells with the highest reflectivity are at the mature-to-late stages of development, with downdrafts associated with heavier precipitation, whereas cells in the initial

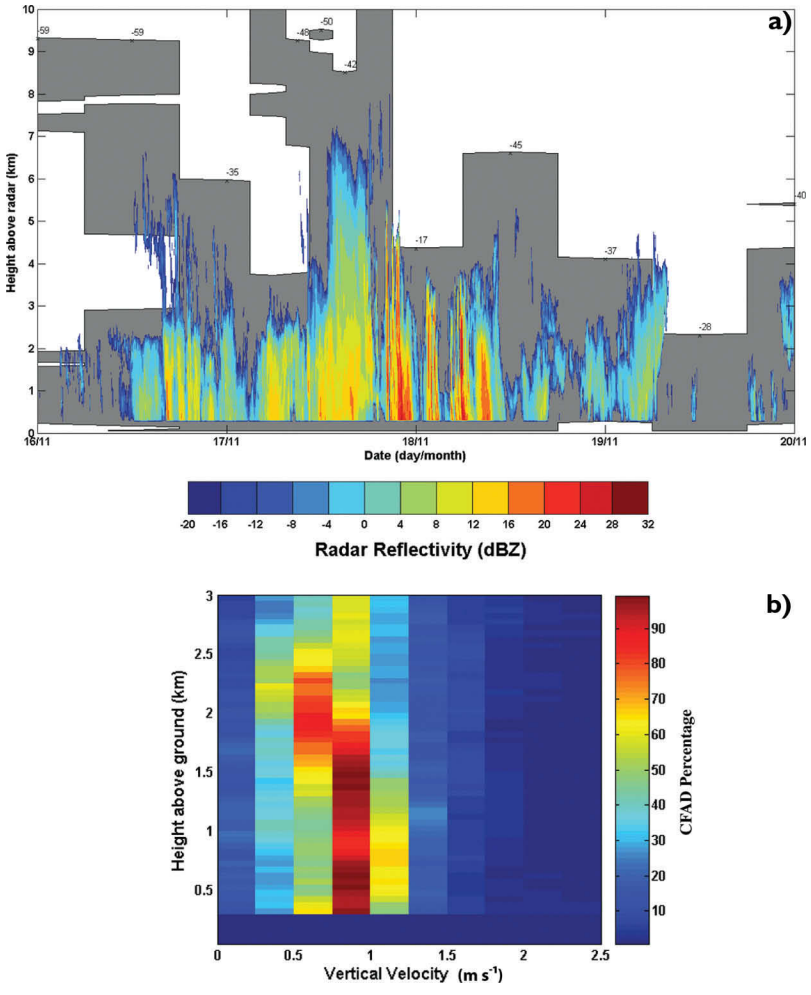

Fig. 9. (a) Iqaluit surface-based radar reflectivity as a function of height and time for the period 16–20 Nov 2007. Also shown in gray is the presence of clouds based on sounding information. The numbers at the cloud top are cloud-top temperatures. (b) Normalized CFAD percentages (color shades) for vertical fall speed as a function of height for the period 16–20 Nov 2007. Notice that data are only valid above 0.3 km AGL

stages of development, with larger upward vertical velocities, show lower reflectivity/precipitation. Near-surface air temperatures were −9° to −10°C, with moderate surface 700-hPa westerly winds (11–15 m s^{-1}) as measured by dropsondes. The combination of cold atmospheric temperatures and relatively warmer ocean temperatures (near −1°C) generated the low-level convective instability (not shown). Equivalent potential temperature and humidity cross sections from dropsondes (Fig. 11) clearly reveal a well-mixed boundary layer up to 2 km MSL (or ~800 hPa), with a dry, shallow inversion just above 2 km MSL capping the convection. The inversion is hypothesized to be caused by midlevel subsidence as an upper weak ridge approached Hudson Strait (not shown). The air–sea temperature differences and horizontal wind speeds are smaller than in other studies (e.g., Renfrew and Moore 1999) and are most likely the primary reason for longer wavelength roll vortex structures; however, the boundary layer structure for this case is similar to that found in other studies (e.g., Atkinson and Zhang 1996; Renfrew and Moore 1999). The depth of the convection/instability, along with a moderate westerly flow and a low-level weak trough that traversed Baffin Island, caused the unexpected highly rimed snowfall in Iqaluit. More detailed analysis, using radar Doppler velocities and cloud microphysical characteristics, including cloud liquid water contents, is ongoing.

Cloudsat observations. Cloudsat-derived single-layer clouds occurred 65% of the time, on average, over southern Baffin Island during the STAR period (60% in October, 71% in November; Fig. 12). Multilayered clouds were less frequent but remained evident, with a 20% occurrence, whereas cloud-free skies accounted for the remaining 15% of the study.

High tops (>7 km MSL) were also a common feature of the clouds over southern Baffin Island, occurring 33% of the time in October when clouds were observed (Fig. 12). Overall for the months of October and November, cloud tops were variable, although low-level cloud tops (1000–3000 m MSL) became more dominant in November and high-level cloud tops greatly diminished in frequency.

Several of these features can be easily observed in a storm system that passed through the region on 17 November 2007 (Fig. 13). The figure shows that MODIS-derived cloud-top temperatures were −60°C across a broad area within and around the Cloudsat track, in conjunction with vertical radar reflectivity from Cloudsat. Cloud-top heights ranged from 7 to 11 km with lower cloud tops in the southern portion of the storm. The storm is also observed largely as a single-layer cloud system with intermittent regions of layering. Sublimation regions (indicated in Fig. 13) produced significant cooling in the sector

of the storm that fed back into the storm's evolution, as found in other high-latitude cloud systems (e.g., Szeto et al. 1997). Radar bright banding caused by melting (shown in Fig. 13) was also a significant feature for this storm over the ocean. Ongoing work is focusing on aircraft cloud microphysical and radar measurements to validate Cloudsat data, on this mission as well as on others, for the first time in this region of the Arctic.

Blowing snow. Special blowing snow instruments were deployed at the Iqaluit Environment Canada facility (see "Weather station mesonet" and "Special surface observations" sections) to investigate threshold wind speeds for blowing snow and particle size distributions in association with visibility reductions. A brief description of some of these results is given later. On the basis of particle counter measurements during STAR, number fluxes and particles per square meter per second (v) at a height of 1 m were compared to the 10-m wind speed measurements (U_{10}) in Figs. 14a–d for four blowing snow episodes. There were more than 30 blowing snow episodes throughout the course of the study; these four are chosen as a sample. The figures show a threshold wind speed for the initiation of blowing snow between 7 and 10 m s^{-1}, expectedly somewhat larger than observations over smooth sea

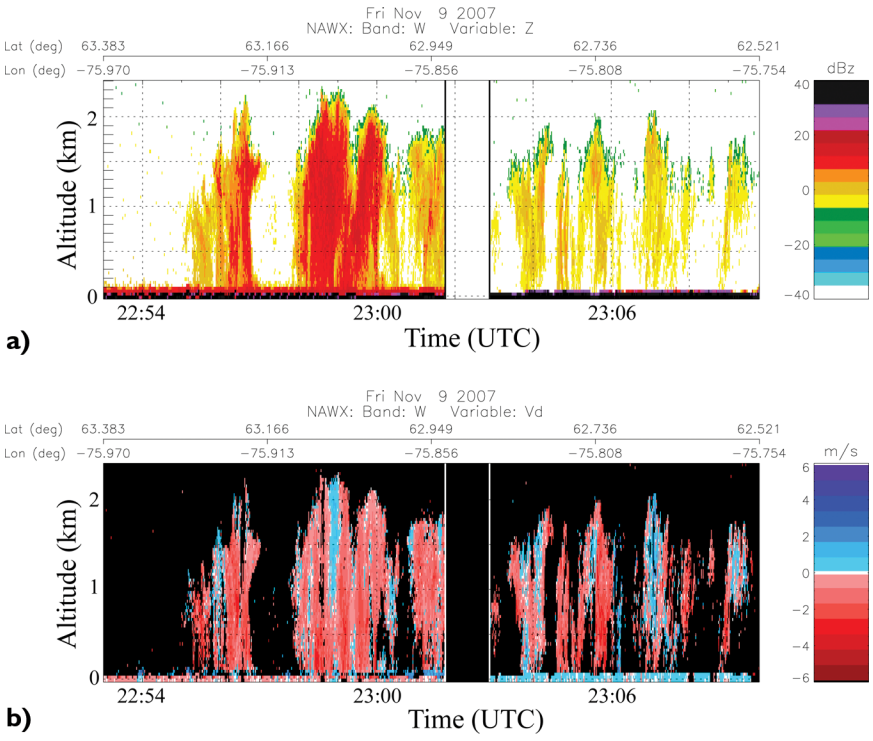

Fig. 10. IOP9 (roll vortices) W-band downward-looking aircraft radar data for the upper-level north–south leg in Fig. 5c (perpendicular to the westerly surface, 700-hPa flow): (a) *Z* (dBZ) and (b) Doppler velocity (V_d) (m s^{-1}) showing convective tower structures. The *Z* (dBZ) and V_d color scales are shown on the right of each figure, respectively. Blue (red) shades for V_d indicate upward (downward) vertical velocity [away from surface (toward the surface)]. The *y* axis is vertical distance above sea level (km), and the *x* axis is time (UTC), increasing from left to right (approximately north–south for this flight). Each minute in time is approximately 5.4 km in horizontal distance, with an average aircraft speed of 90 m s^{-1}. The latitude and longitude scale is shown at the top of each figure.

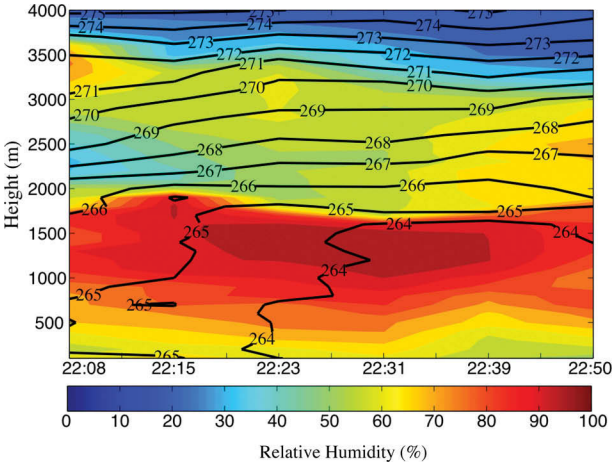

Fig. 11. IOP9 (roll vortices) dropsonde vertical cross sections between 2208 and 2250 UTC 9 Nov (high-level east–west outbound leg into Hudson Strait shown in Fig. 5c) of contoured equivalent potential temperature (θ_e in K) and relative humidity (%; shaded). The *x* axis shows the times of the cross sections (UTC), and the *y* axis shows MSL height (m). Each minute in time is approximately 5.4 km in horizontal distance, with an average aircraft speed of 90 m s^{-1}. The cross section is oriented parallel to the mean low-level (surface to 700 hPa) flow, which was westerly between 11 and 15 m s^{-1}.

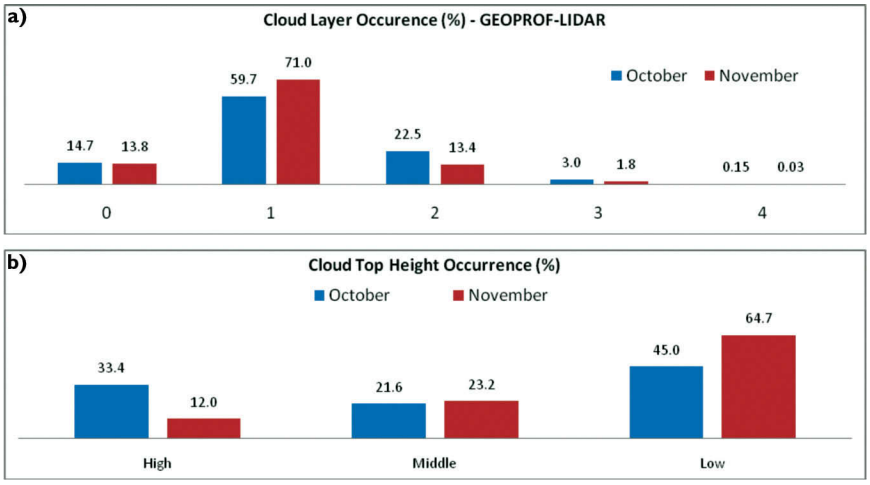

Fig. 12. (a) Cloudsat-derived frequency distribution of cloud layers occurring over southern Baffin Island for October and November 2007. (b) Cloud-top height occurrence over southern Baffin Island for October and November 2007 of high clouds (>7 km), middle clouds (3–7 km), and low clouds (1–3 km).

ice (e.g., Huang et al. 2008). Previous studies (e.g., Mann et al. 2000) have demonstrated hysteresis, with the value of the threshold wind speed showing dependence on the history of the blowing snow event. Once saltation begins, and the bonds of particles at the surface are broken, saltating particles then further erode the surface, providing more loose particles and lowering the threshold wind speed required to sustain blowing snow. In Figs. 14a–d, a distinction is made between measurements before (red lines with "+") and after (blue lines with "×") the peak value of v is reached. In Fig. 14a, which describes 18 November 2007, a hysteresis is seen, with wind speeds near 10 m s^{-1} required to initiate blowing snow. After approximately five hours of continuous blowing snow, the same number of fluxes ($2 \times 10^6 < v < 6 \times 10^6\,m^{-2}\,s^{-1}$) is maintained by lower wind speeds. However, this effect is not seen in other blowing snow episodes, including the three shown in Figs. 14b–d). In these episodes, very little difference is seen between the start and the end of the episode. This difference is likely due to relatively high temperatures (–1°C) and humidity (99% with respect to ice) that occurred soon after a snowfall ended at approximately 1700 UTC 17 November. This would result in strong bonding of snow particles at the surface, requiring a higher wind

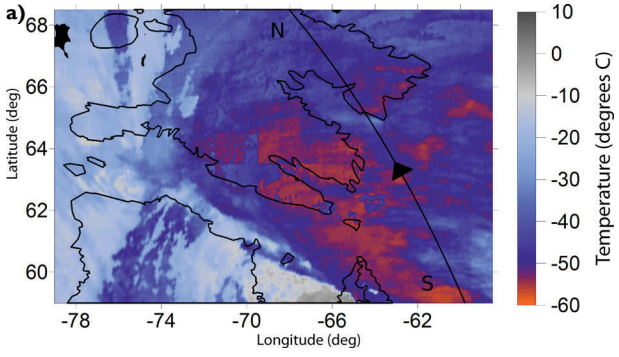

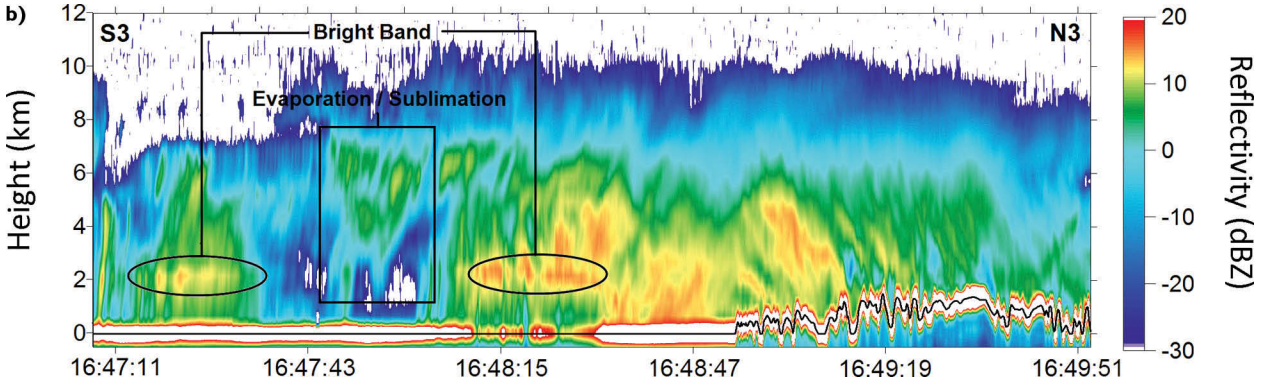

Fig. 13. IOP11 17 Nov storm images of (a) 1645 UTC MODIS and (b) ~1647–1650 UTC Cloudsat radar. The Cloudsat track (roughly south–north) is indicated by the black line in (a) and the corresponding Cloudsat radar reflectivity along the same track is shown in (b). The temperature scale in (a) is given in degrees Celsius for cloud-top temperature, whereas the reflectivity scale in (b) is in decibels. In (a) the *y* and *x* axes are latitude and longitude, respectively. In (b) the *y* axis is height (km) and the *x* axis is time (HH:MM:SS).

speed to break the bonds and initiate blowing snow. Conversely, the temperatures preceding the blowing snow in the episodes in Figs. 14b,c were in the range of $-30 < T < -20$°C, whereas temperatures preceding the episode shown in Fig. 14d were approximately −11°C.

Blowing snow is generally associated with a reduction in visibility, as measured by the meteorological optical range (MOR). Huang et al. (2008) found that the MOR relates to the blowing snow particle number density N and particle size (measured at the same height) as

$$\mathrm{MOR} = \frac{7.84}{N\pi\bar{d}_a^2} \qquad (1)$$

where d_a is the cross-sectional area-weighted mean particle diameter. Over a sea ice surface in Franklin Bay, Northwest Territories, Huang et al. (2008) found $d_a \approx 100\ \mu$m, with MOR and number density measured at a height of 1.5 m.

The MOR, measured at a height of 2 m, was compared to the number density calculated as $N = v_2/U_2$ using the 2-m particle counter (for v_2) and the 2-m cup anemometer (for U_2) when U_{10} (wind speed at 10 m) > 6 m s^{-1} without precipitating snow or ice crystals. A least squares fit to the data gives a cross-sectional area-weighted mean particle diameter of $d_a = 109\ \mu$m with $R^2 = 0.83$. This is close to the diameter of $d_a \approx 100\ \mu$m found by Huang et al. (2008).

This analysis is critical for better understanding blowing snow processes with respect to severe visibility reductions during these events, as well as for improving blowing snow models. An analysis of more events and modeling applications is ongoing.

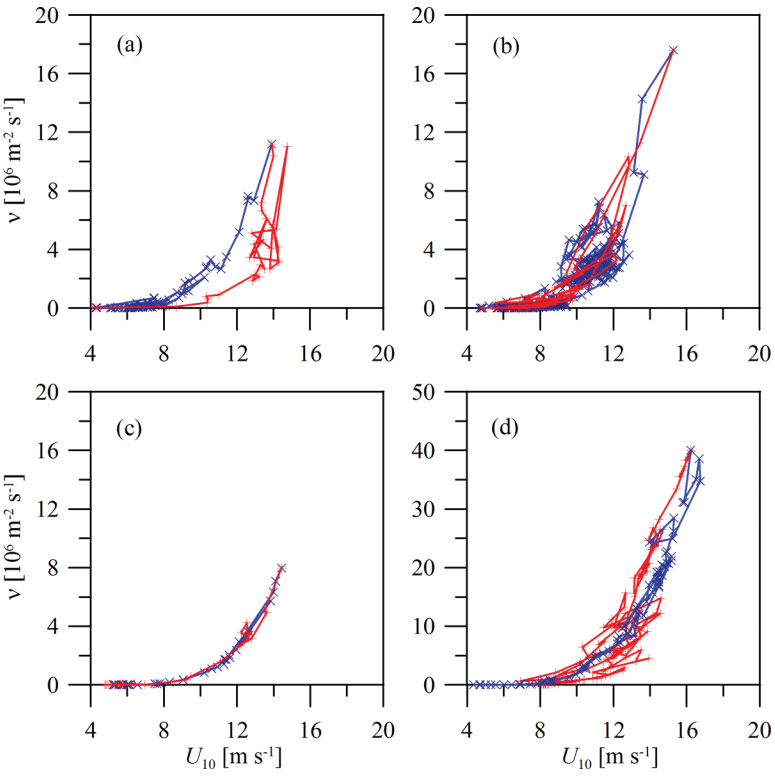

FIG. 14. Blowing snow number flux v at a height of 1 m compared to U_{10} for four blowing snow episodes: (a) 18–19 Nov 2007; (b) 16–19 Feb 2008; (c) 18 Mar 2008; and (d) 22–24 Mar 2008. Measurements leading up to the peak value are shown in red (+), whereas measurements after the peak value are shown in blue (×). Notice the different y-axis scale in (d).

COMMUNITY INTERACTIONS. A major goal of the STAR network is to interact with local communities. During the field project, a public "kickoff" was held in Iqaluit with local northern dignitaries, members of Parliament, and media in attendance. The gathering was extremely well received, and the significance of extreme weather to northern communities was strongly voiced, as was the hope that STAR would make a significant contribution to a better understanding of storms in the region. The day ended with a tour of the research aircraft and a public STAR presentation made by project leads. Local Iqaluit students were given tours of the STAR instrumentation and Environment Canada facility, to not only educate the students, but to offer local career options within Environment Canada (e.g., upper-air and instrumentation technicians).

An ongoing STAR project is focusing on improving understanding of hazardous weather in Iqaluit through the involvement of community residents and organizations in identifying and analyzing 1) the effects of hazardous weather on residents and their social, economic, and cultural activities; 2) ways in which residents adapt to hazardous weather and related events; 3) ways in which residents prepare for these events; 4) ways in which residents recognize these events in advance; and 5) the effectiveness and reliability of traditional and science-based weather forecasts for community residents. There is hope that this research will also shed light on community-specific adaptations to hazardous weather and the ways in which certain segments of the population are more vulnerable to weather hazards than others. Unfortunately, no results are yet available because

data are still in the process of being gathered for this project through community visits and consultations; however, one of the important legacies of STAR will be the results that will be available in the near future.

STAR researchers and students will visit several communities over the next year to hold public seminars and small workshops to disseminate STAR results in a nontechnical process. STAR is also looking into producing educational material (i.e. visual presentations, reading material, and lab exercises) at the college level for use by the Nunavut Research Institute and other northern educational institutions.

DATA MANAGEMENT. As with any field project, data management is a major issue. STAR has invoked the IPY metadata format standard for its long-term data archive and has fully implemented this protocol. It was decided that STAR could take advantage of the IPY infrastructure and data management guidelines to ensure its longevity for future research. Once the Canadian IPY data repository location has been determined, this will be a likely choice to archive STAR datasets in the future.

Once STAR is complete in winter 2010, the compiled datasets will become available to the national and international research communities via the National Center for Atmospheric Research (NCAR) data archive (in process). Until that time and thereafter, STAR researchers welcome other Canadian and international researchers to collaborate on the analysis of these datasets.

CONCLUDING REMARKS. The STAR field project was the first of its kind in the eastern Canadian Arctic, providing a unique dataset for better understanding severe arctic storms and associated weather hazards. The field phase was conducted between 10 October and 30 November 2007 and in February 2008. Sixteen IOPs were conducted, covering a variety of weather situations and mesoscale phenomena over the region. The results of the project are expected to improve our current understanding of arctic weather and to contribute to its improved prediction.

One of the more important tasks includes developing a conceptual model of storms and associated phenomena in the region. A better understanding of the organization, structure, and mesoscale features (where applicable) of weather events is critical for improving operational forecasting and for providing a context for future events. Another important task is to evaluate operational and model forecasts of the events to examine where improvements need to be made and under what circumstances. The suite of STAR data will be used to address these issues, and, through case study analysis, target specific modeling activities and experiments to investigate the physical processes that need to be improved in the models. Further analysis of high-resolution modeling from GEM-LAM and MM5 will be a primary activity for STAR.

Although STAR occurred over a limited region of the Arctic, the physiographic features of its location are typical of many other parts of the Arctic; thus, the physical understanding that is gained during STAR will be widely applicable. The STAR dataset will also be a legacy for future projects in the arctic region, including future IPY projects.

ACKNOWLEDGMENTS. This research and network is primarily funded through a network grant from the Canadian Foundation for Climate and Atmospheric Sciences (CFCAS). We also acknowledge the financial and equipment infrastructure support from the Natural Sciences and Engineering Research Council (NSERC), Canada Foundation for Innovation (CFI), and the Northern Scientific Training Program (NSTP). We are grateful to the reviewers of this article, who provided excellent feedback during the review process. The authors wish to thank the many collaborators who provided significant contributions: Environment Canada—Meteorological Research Division (MRD), Climate Research Division (CRD), Hydrometeorological and Arctic Lab (HAL), Prairie and Arctic Storm Prediction Centre (PASPC), and the Weather and Environmental Monitoring Section; the National Research Council—Flight Research Lab; the Nunavut Research Institute (NRI); Qulliq Energy Corporation; and Indian and Northern Affairs Canada (INAC). The National Research Council (NRC) and Environment Canada aircraft personnel are to be commended for their work on the project. A special thank you to Jim Young and Steve Brady (MRD) for Doppler radar and communications installation; Khalid Malik (York University) for field equipment deployment; Melanie Howell (Iqaluit resident) for field logistics assistance; and Jamal Shirley (NRI) and the NRI students for help with installing the sea ice station and its data collection. Appreciation is also extended to Nyree Sharp for assisting with editing the final manuscript.

REFERENCES

Atkinson, B. W., and J. W. Zhang, 1996: Mesoscale shallow convection in the atmosphere. *Rev. Geophys.*, **34,** 403–431.

Barber, D. G., J. M. Hanesiak, W. Chan, and J. Piwowar, 2001: Sea-ice and meteorological conditions in north-

ern Baffin Bay and the North Water Polynya between 1979 and 1996. *Atmos.–Ocean,* **39,** 343–359.

Brown, T., and J. W. Pomeroy, 1989: A blowing snow particle detector. *Cold Reg. Sci. Technol.,* **16,** 167–174.

Cavalieri, D., C. Parkinson, P. Gloersen, and H. J. Zwally, 2008: Sea ice concentrations from Nimbus-7 SMMR and DMSP SSM/I passive microwave data, 1980–2005. National Snow and Ice Data Center, Boulder, CO, digital media. [Available online at http://nsidc.org/data/nsidc-0051.html.]

Curry, J., 2001: Introduction to special section: FIRE Arctic Clouds Experiment. *J. Geophys. Res.,* **106** (D14), 14985–14987.

Deser, C., J. E. Walsh, and M. S. Timlin, 2000: Arctic sea ice variability in the context of recent atmospheric circulation trends. *J. Climate,* **13,** 617–633.

Fargey, S., J. Hanesiak, G. Liu, J. Gilligan, and R. Stewart, Eds., 2008: The Storm Studies in the Arctic (STAR) data report. Centre for Earth Observation Science Rep., 75 pp.

Goodison, B. E., 1978: Accuracy of Canadian snow gauge measurements. *J. Appl. Meteor.,* **17,** 1542–1548.

——, and D. Yang, 1995: *In-situ* measurements of solid precipitation in high latitudes: The need for correction. *Proc. Workshop on the ACSYS Solid Precipitation Climatology Project*, Reston, VA, World Climate Research Programme, WCRP-93, WMO/TD 793, 3–17.

——, P. Y. T. Louie, and D. Yang, 1998: WMO solid precipitation measurement intercomparison: Final report. World Meteorological Organization, Instruments and Observing Methods Rep. 67, WMO/TD 872, 318 pp.

Gordon, M., and P. A. Taylor, 2009a: Measurements of blowing snow, Part I: Particle shape, size distribution, velocity, and number flux at Churchill, Manitoba, Canada. *Cold Reg. Sci. Technol.,* **55,** 63–74, doi:10.1016/j.coldregions.2008.05.001.

——, and ——, 2009b: The Electric Field During Blowing Snow Events. *Bound.-Layer Meteor.,* **130,** 97–115, doi:10.1007/s10546-008-9333-7.

——, S. Savelyev, and P. A. Taylor, 2009: Measurements of blowing snow, Part II: Mass and number density profiles and saltation height at Franklin Bay, NWT, Canada. *Cold Reg. Sci. Technol.,* **55,** 75–85, doi:10.1016/j.coldregions.2008.07.001.

Hanesiak, J. M., and R. E. Stewart, 1995: The mesoscale and microscale structure of a severe ice pellet storm. *Mon. Wea. Rev.,* **123,** 3144–3162.

——, and X. Wang, 2005: Adverse weather trends in the Canadian Arctic. *J. Climate,* **18,** 3140–3156.

——, R. E. Stewart, K. K. Szeto, D. R. Hudak, and H. Leighton, 1997: The structure, water budget, and radiational features of a high-latitude warm front. *J. Atmos. Sci.,* **54,** 1553–1573.

Hassol, S. J., 2004: *Impacts of a Warming Arctic: Arctic Climate Impact Assessment.* Cambridge University Press, 139 pp.

Hoskins, B. J., and K. I. Hodges, 2002: New perspectives on the Northern Hemisphere winter storm tracks. *J. Atmos. Sci.,* **59,** 1041–1061.

Huang, Q., J. M. Hanesiak, S. Savelyev, T. Papakyriakou, and P. A. Taylor, 2008: Visibility during blowing snow events over arctic sea ice. *Wea. Forecasting,* **23,** 741–751.

Hudak, D. R., R. E. Stewart, G. W. K. Moore, and E. T. Hudson, 1995: Synoptic considerations of storms in the southern Beaufort Sea—Expectations for BASE. Preprints, *Fourth Conf. on Polar Meteorology and Oceanography*, Dallas, TX, Amer. Meteor. Soc., 234–237.

——, B. Currie, R. E. Stewart, P. Rodriguez, J. Burford, N. Bussieres, and B. Kochtubajda, 2004: Weather systems occurring over Fort Simpson, Northwest Territories, Canada, during three seasons of 1998/99. Part 1: Cloud features. *J. Geophys. Res.*, **109**, D22108, doi: 10.1029/2004JD004876.

Hudson, E., D. Aihoshi, T. Gaines, G. Simard, and J. Mullock, 2001: Weather of Nunavut and the Arctic. NAV Canada Rep., 246 pp.

Intihar, M. R., and R. E. Stewart, 2005: Extratropical cyclones and precipitation within the Canadian Archipelago during the cold season. *Arctic,* **58,** 162–174.

Joly, A., and Coauthors, 1999: Overview of the field phase of the fronts and Atlantic Storm-Track EXperiment (FASTEX) project. *Quart. J. Roy. Meteor. Soc.,* **125,** 3131–3163.

Kaplan, M. L., Y. L. Lin, J. J. Charney, K. D. Pfeiffer, D. B. Ensley, D. S. DeCroix, and R. P. Weglarz, 2000: A terminal area PBL prediction system at Dallas–Fort Worth and its application in simulating diurnal PBL jets. *Bull. Amer. Meteor. Soc.,* **81,** 2179–2204.

Knippertz, P., U. Ulbrich, and P. Speth, 2000: Changing cyclones and surface wind speeds over the North Atlantic and Europe in a transient GHG experiment. *Climate Res.,* **15,** 109–122.

Mahapatra, P. R., and D. S. Zrnic, 1991: Sensors and Systems to Enhance Aviation Safety against Weather Hazards. *Proc. IEEE,* **79,** 1234–1267.

Mann, G. W., P. S. Anderson, and S. D. Mobbs, 2000: Profile measurements of blowing snow at Halley, Antarctica. *J. Geophys. Res.,* **105** (D19), 24 491–24 508.

Martin, R. E., and G. W. K. Moore, 2005: Transition of a synoptic system to a polar low via interaction with the orography of Greenland. *Tellus,* **58A,** 236–253.

McCabe, G. J., M. P. Clark, and M. C. Serreze, 2001: Trends in Northern Hemisphere surface cyclone frequency and intensity. *J. Climate,* **14,** 2763–2768.

Moore, G. W. K., 2006: Reduction in seasonal sea ice concentration surrounding southern Baffin Island 1979–2004. *Geophys. Res. Lett.,* **33,** L20501, doi:10.1029/2006GL027764.

Morison, J., K. Aagaard, and M. Steele, 2000: Recent environmental changes in the Arctic: A review. *Arctic,* **53,** 359–371.

Nawri, N., and R. E. Stewart, 2006: Climatological features of orographic low-level jets over Frobisher Bay. *Atmos.–Ocean,* **44,** 397–413.

——, and ——, 2008: Channelling of high-latitude boundary-layer flow. *Nonlinear Processes Geophys.,* **15,** 33–52.

Neilsen, D., 2007: The City of Iqaluit's climate change impacts, infrastructure risks, and adaptive capacity project. City of Iqaliuit Rep., 88 pp.

NOAA, cited 2007: Hurricane Noel advisory archive. [Available online at www.nhc.noaa.gov/archive/2007/NOEL.shtml.]

NTI, 2001: Elder's conference on climate change: Final report. Nunavut Tunngavik Incorporated Rep., 36 pp.

Ozawa, H., K. Goto-Azuma, K. Iwanami, and R. M. Koerner, 1998: Cirriform rotor cloud observed on a Canadian Arctic ice cap. *Mon. Wea. Rev.,* **126,** 1741–1745.

Prinsenberg, S., 1986: On the physical oceanography of Foxe Basin. *Canadian Inland Seas,* I. P. Martini, Ed., Elsevier, 217–236.

Rasmussen, E. A., J. Turner, and P. F. Twitchell, 1993: Report of a workshop on applications of new forms of satellite data in polar low research. *Bull. Amer. Meteor. Soc.,* **74,** 1057–1073.

Renfrew, I. A., and G. W. K. Moore, 1999: An extreme cold-air outbreak over the Labrador Sea: Roll vortices and air–sea interaction. *Mon. Wea. Rev.,* **127,** 2379–2394.

——, and Coauthors, 2008: The Greenland Flow Distortion Experiment. *Bull. Amer. Meteor. Soc.,* **89,** 1307–1324.

Roberts, E., and R. E. Stewart, 2008: On the occurrence of freezing rain and ice pellets over the eastern Canadian Arctic. *Atmos. Res.,* **89,** 93–109.

——, N. Nawri, and R. E. Stewart, 2008: On the storms passing over southern Baffin Island during autumn 2005. *Arctic*, **61,** 309–321.

Savelyev, S. A., M. Gordon, J. Hanesiak, T. Papakyriakou, and P. A. Taylor, 2006: Blowing snow studies in CASES (Canadian Arctic Shelf Exchange Study) 2003–04. *Hydrol. Processes,* **20,** 817–827.

Serreze, M. C., and Coauthors, 2000: Observational evidence or recent change in the northern high-latitude environment. *Climatic Change,* **46,** 159–207.

Smith, C. G., 2008: Correcting the wind bias in snowfall measurements made with a Geonor T-200B precipitation gauge and alter wind shield. *CMOS Bull.,* **36,** 162–167.

Stewart, R. E., 1991: Canadian Atlantic Storms Program: Progress and plans of the meteorological component. *Bull. Amer. Meteor. Soc.,* **72,** 364–371.

——, and Coauthors, 1998: The Mackenzie GEWEX Study: The water and energy cycles of a major North American River basin. *Bull. Amer. Meteor. Soc.,* **79,** 2665–2683.

——, J. E. Burford, D. R. Hudak, B. Currie, B. Kochtubajda, P. Rodriguez, and J. Liu, 2004: Weather systems occurring over Fort Simpson, Northwest Territories, Canada, during three seasons of 1998–99: 2. Precipitation features. *J. Geophys. Res.,* **109,** D22109, doi: 10.1029/2004JD004929.

Stone, D. A., A. J. Weaver, and F. W. Zwiers, 2000: Trends in Canadian precipitation intensity. *Atmos.–Ocean,* **38,** 321–347.

Szeto, K. K., R. E. Stewart, and J. M. Hanesiak, 1997: High-latitude cold season frontal cloud systems and their precipitation efficiency. *Tellus,* **49A,** 439–454.

Zhang, X., J. E. Walsh, J. Zhang, U. S. Bhatt, and M. Ikeda, 2004: Climatology and interannual variability of arctic cyclone activity: 1948–2002. *J. Climate,* **17,** 2300–2317.